available at www.sciencedirect.com

ScienceDirect

www.elsevier.com/locate/brainres

BRAIN RESEARCH

Research Report

Intracerebroventricular administration of Shiga toxin type 2 induces striatal neuronal death and glial alterations: An ultrastructural study

Jorge Goldstein[a,*], *César Fabián Loidl*[b], *Virginia Pistone Creydt*[a], *Javier Boccoli*[a], *Cristina Ibarra*[a]

[a]*Laboratorio de Fisiopatogenia, Departamento de Fisiología, Facultad de Medicina, Universidad de Buenos Aires, 1121, Argentina*
[b]*Instituto de Biología Celular y Neurociencia "Prof. E. De Robertis", Facultad de Medicina, Universidad de Buenos Aires, Buenos Aires, 1121, Argentina*

ARTICLE INFO

Article history:
Accepted 31 May 2007
Available online 14 June 2007

Keywords:
Shiga toxin 2
Corpus striatum
Intracerebroventricular
Brain injury
Transmission electron microscopy

ABSTRACT

Shiga toxin (Stx) from enterohemorrhagic *Escherichia coli* (STEC) is the main cause of hemorrhagic colitis which may derive to hemolytic–uremic syndrome (HUS). HUS is characterized by acute renal failure, thrombocytopenia and microangiopathic hemolytic anemia. Mortality in the acute stage has been lower than 5% of total affected argentine children with endemic HUS. Common signs of severe CNS involvement leading to death included seizures, alteration of consciousness, hemiparesis, visual disturbances, and brainstem symptoms. The main purpose of the present work was to study the direct involvement of Stx2 in brain cells by intracerebroventricular (i.c.v.) administration of Stx2. Immunodetection of Stx2 was confirmed by immunoelectron cytochemistry in different subsets and compartments of affected caudate putamen cells of corpus striatum. Transmission electron microscopy (TEM) studies revealed apoptotic neurons, glial ultrastructural alterations and demyelinated fibers. The i.c.v. microinfusion was applied for the first time in rats to demonstrate the direct action of Stx2 in neurons and glial cells. The toxin may affect brain neuroglial cells without the involvement of proinflammatory or systemic neurotoxic elements.

1. Introduction

Shiga toxin (Stx) from enterohemorrhagic *Escherichia coli* (STEC) is the main cause of hemorrhagic colitis which may derive to hemolytic–uremic syndrome (HUS) (O'Brien and Kaper, 1998), a triad of events which include: thrombocytopenia, microangiopathic hemolytic anemia, and acute renal failure (Proulx et al., 2001). Argentina is the first country with 400 new cases a year. Mortality in the acute stage has been lower than 5% of total affected argentine children with endemic HUS since 1978 (Repetto, 2005). Children usually die because of severe involvement of the central nervous system (Exeni, 2001; Eriksson et al., 2001; Oakes et al., 2006). Common signs of severe CNS involvement included seizures, alteration of consciousness, hemiparesis,

* *Corresponding author*. Laboratorio de Fisiopatogenia, Departmento de Fisiología, Facultad de Medicina, UBA, Paraguay 2155 piso 7, Ciudad Autónoma de Buenos Aires, 1121, Argentina. Fax: +54 11 4 964 0503.
E-mail address: jogol@fmed.uba.ar (J. Goldstein).

Abbreviations: HUS, hemolytic–uremic syndrome; i.c.v., intracerebroventricular; Stx, Shiga toxin; STEC, Shiga toxin from enterohemorrhagic *Escherichia coli*; TEM, transmission electron microscopy

0006-8993/$ – see front matter © 2007 Elsevier B.V. All rights reserved.
doi:10.1016/j.brainres.2007.05.067

visual disturbances and brainstem symptoms (Siegler, 1994; Gallo and Gianantonio, 1995). Some authors suggested that the origin of CNS pathogenesis by HUS was secondary to metabolic changes: hyponatraemia, azotaemia, hydration disorders or hypertension (Siegler, 1994; Gallo and Gianantonio, 1995). Other authors claimed more for infarction of the brain microvasculature by Stx leading to neurological damage (Taylor et al., 1999; Mizuguchi et al., 2001). And whether Stx2 directly affected brain neuroglial cells is yet to be investigated. To study this issue then the toxin should not pass through brain microvasculature, through the blood–brain barrier (BBB). One way to circumvent the microvasculature is to i.c.v. microinfuse the toxin in a certain brain area. Therefore, does Stx2 possess a direct neurotoxic involvement on brain parenchymal cells? This prompted us to study the role of Stx2 on brain injury.

The studies of brain intoxication produced by Stx were usually performed in animal models of STEC colonic invasion, Stx intraperitoneal (i.p.) or endovenous (e.v.) systemic administrations. In some previous reports, the action of Stx2 in brain was focused on mitomycin-treated mice intragastrically inoculated with the *Escherichia coli* O157:H– strain E32511/HSC (Fujii et al., 1994). In addition, studies with Stx2 administration on animal models for the toxin neuropathogenicity was only performed by e.v. (Fujii et al., 1996; Yamada et al., 1999; Mizuguchi et al., 2001) or intrathecal (Mizuguchi et al., 1996, Fujii et al., 1998) toxin administration in rabbit brains (Fujii et al., 1996, 1998; Mizuguchi et al., 1996, 2001; Yamada et al., 1999). E.v. administration caused a selective damage of neurons seen in the lower layers of the cerebellar and cerebral cortex, midbrain and spinal cord and in a later phase involvement of pathological changes of blood vessels (Mizuguchi et al., 1996). However, immunodetection of the toxin was not shown in the brain parenchyma; it was rather observed on blood vessels' walls. Other MRI studies performed in rabbits showed brain lesions in the hypothalamus, hippocampus, brain stem, medulla (Fujii et al., 1996) and cerebellum after e.v. Stx2 or intrathecal injection (Fujii et al., 1998). Although this technique proved to be an efficient tool to detect brain lesions, the topographic distribution of the toxin within an affected brain area and its toxic influence at the cell level could not be determined. This technique therefore is not suitable to observe the action of Stx at the cell level.

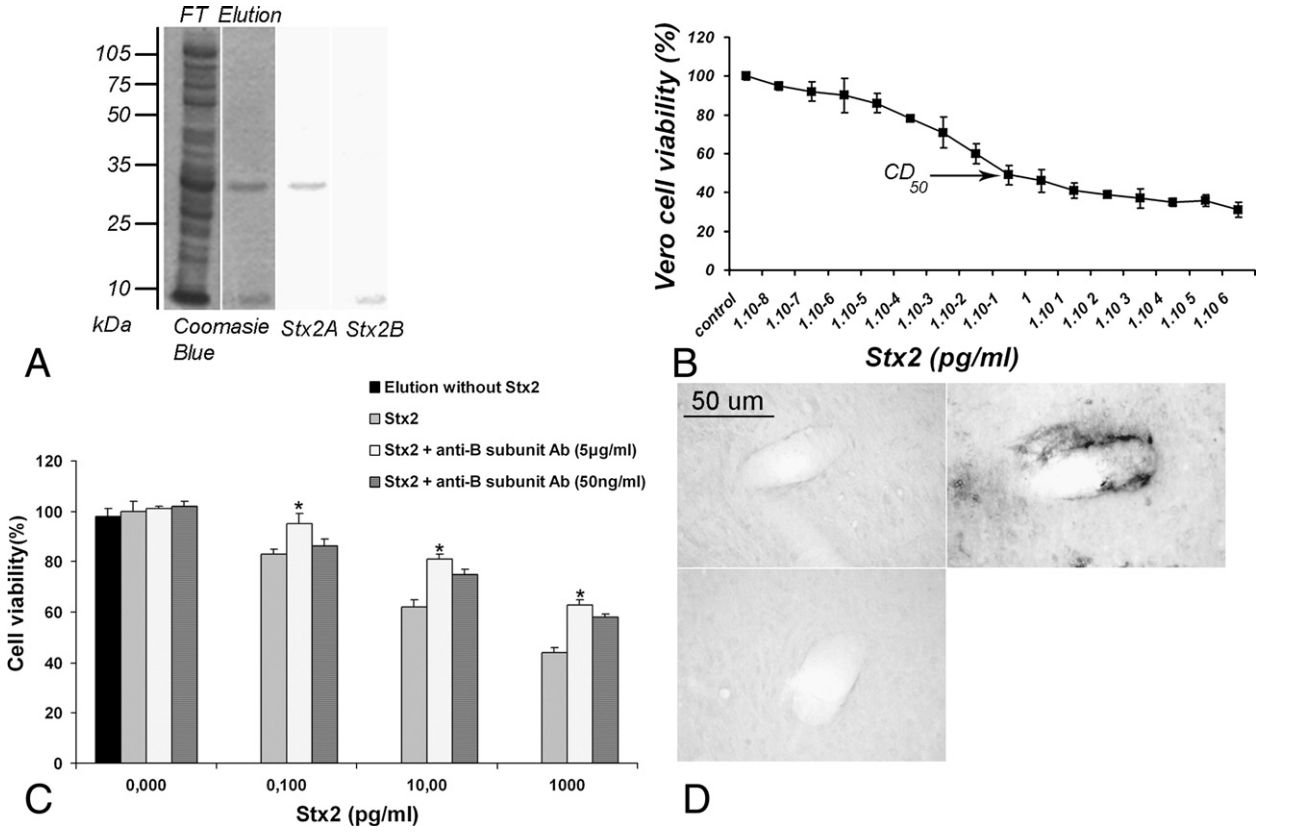

Fig. 1 – Stx2 obtained by affinity chromatography purification was cytotoxic to Vero cells and passed the blood–brain barrier (BBB). An elution that contained Stx2 was analyzed on a SDS–PAGE electrophoretic gel revealing two bands that corresponded to the A and B subunits of Stx2 on Coomassie blue staining (A); these bands were confirmed by WB (A). (FT: flow through). The Stx2 cytotoxic capacity was confirmed on a Vero monolayer cell culture (B). Preincubation of the toxin with increasing concentrations of the monoclonal anti-Stx2B antibody resulted in a significant increase in Vero cell viability in a dose–response manner (C). In B and C, data are reported as means ± S.E.M. of at least three triplicate experiments. *$P<0.05$ (ANOVA). Intraperitoneal Stx2 administration showed that the toxin was able to pass the blood–brain barrier (D); Stx2 immunolocalization was confined to parenchymal brain cells near perivascular spaces (right panel). In the above left panel (D) the isotype control shows non-specific immunoreaction, while a negative control is shown by omitting the primary antibody in the below panel.

The present work shows the first animal model of i.c.v. administration of Stx2 as far as we know. Also, this is the first pathologic brain model by Stx2 administration performed in rats. The i.c.v. technique allows to microinfuse the toxin in specific brain areas of interest by using a stereotaxic frame. To avoid tissue damage, we placed the cannula between the third

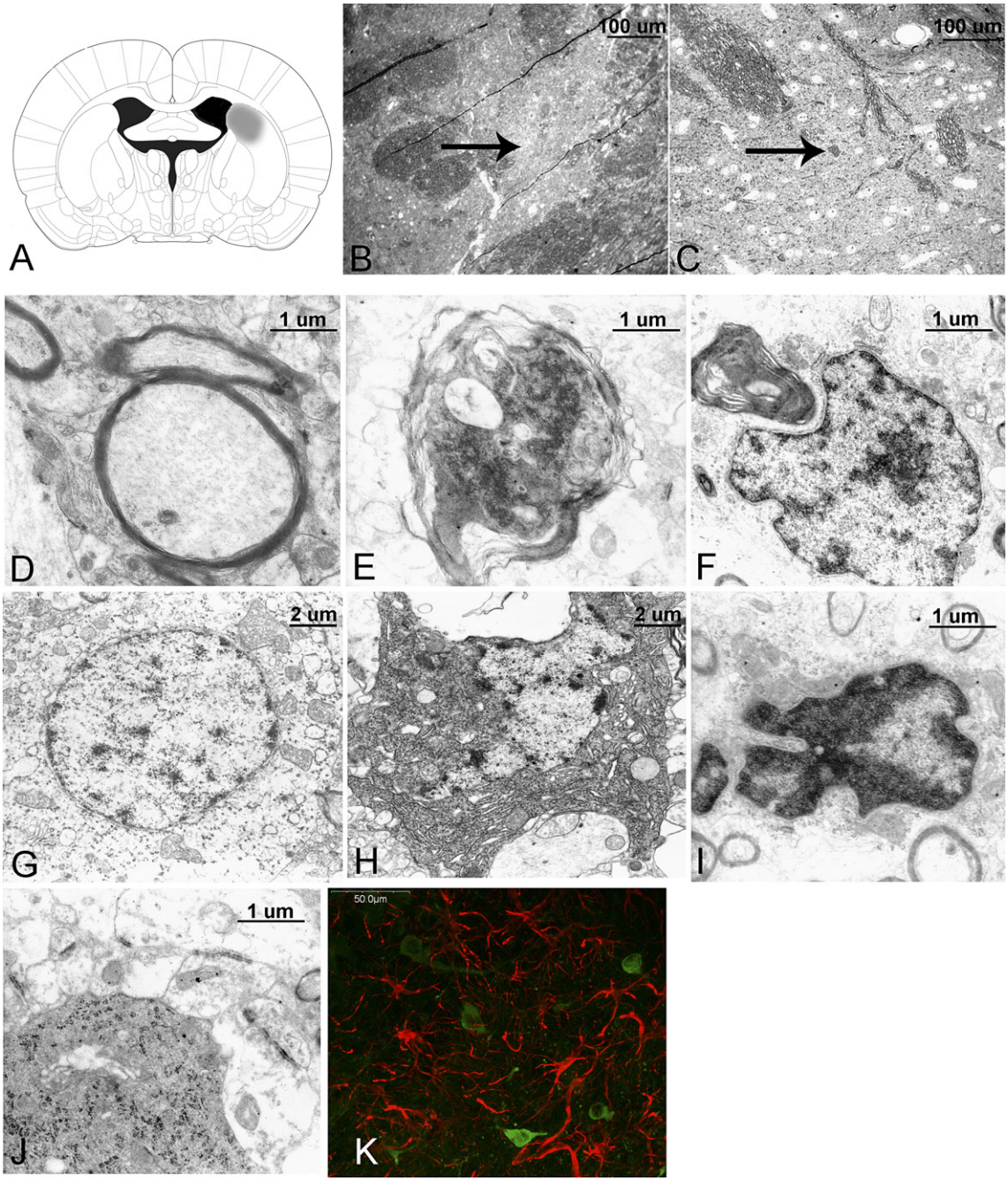

Fig. 2 – I.c.v. administration of Stx2 altered the ultrastructure of fibers and caused neuronal death from dorsal caudate putamen corpus striatum. Electron microphotographs show the direct effect of Stx2 in corpus striatum neurons. The area observed in this study is located in the dorsal caudate putamen from the rat corpus striatum (A) shown in gray. Blue toluidine staining for brain i.c.v. administration of vehicle or Stx2 (B, C respectively) was previous performed to choose the precise affected area in this subregion. In low magnification, affected neurons by i.c.v. Stx2 treatment are observed in contrast and in irregular shape (arrow, C), while this is not observed in neurons in the vehicle control (arrow, B). The selected tissue was further processed for TEM (D–J). Panel E shows a demyelinated and hypertrophic axon. A normal axon from a brain i.c.v. microinfused with vehicle (D). An astrocyte next to a demyelinated fiber (F). Neuronal bodies at different degeneration stages (H–J). A normal neuron from a brain which was i.c.v. microinfused with a vehicle (G). Neurodegenerative details are in the results. I.c.v. Stx2 microinfusion shows Stx2 immunolocalization to neurons (green) and astrocytes (red) (K). Some astrocytes processes are in contact with Stx2 positive neurons. (For interpretation of the references to colour in this figure legend, the reader is referred to the web version of this article.)

and lateral ventricles, from which it contacts the dorsal corpus striatum. This is very different from i.p. or e.v. toxin administration because the distance of delivery is far to assume direct effects of the toxin in the brain. It is known that the induction of systemic pro-inflammatory responses by Stx works synergistically (Stricklett et al., 2002). Therefore the i.c.v. technique enables us to study the direct effect of the toxin in corpus striatum disregarding the involvement of systemic secondary mediators.

Neurological complications (coma, hemiparesis, abnormal and choreoathetoid movements, dystonic posture, alteration of consciousness) found in humans by HUS included disorders in the basal ganglia (Barnett et al., 1995). This area that primarily regulates the initiation of movement was mainly involved in HUS patients that suffered from hemiparesis, seizures, coma, altered mental state or tremor (Steinborn et al., 2004; Barnett et al., 1995). Therefore, in light of the preceding data, the direct action of Stx2 in rat brain corpus striatum results of particular interest to us.

As a novel finding, we present a detailed ultrastructural study of the Stx2 action when is i.c.v. administered in the rat brain. Apoptotic neurons observed by TEM, neuronal Stx2 immunoelectron detection, and pathological ultrastructural alterations of astrocytes and oligodendrocytes are observed in this work.

2. Results

2.1. *The Stx2 obtained by affinity chromatography is cytotoxic to Vero cells and is BBB-diffusible*

In order to i.c.v. administrate a pure Stx2 elution into the brain, we passed the supernatant cell culture that produced Stx2 through an affinity chromatography column.

This product was analyzed on SDS–PAGE electrophoretic gel (Fig. 1A) that revealed two bands that corresponded to A and B subunits Stx2 molecular weights on Coomassie staining; these bands were corroborated by WB (Fig. 1A). We next found that 0.55 pg/ml of this Stx2 elution was enough to kill 50% of a Vero monolayer cell culture (CD_{50} dose) (Fig. 1B) using a standardized procedure (Karmali et al., 1985). This effect was neutralized by the preincubation of an anti subunit B monoclonal antibody (Fig. 1C), performed by an established method (Pistone Creydt

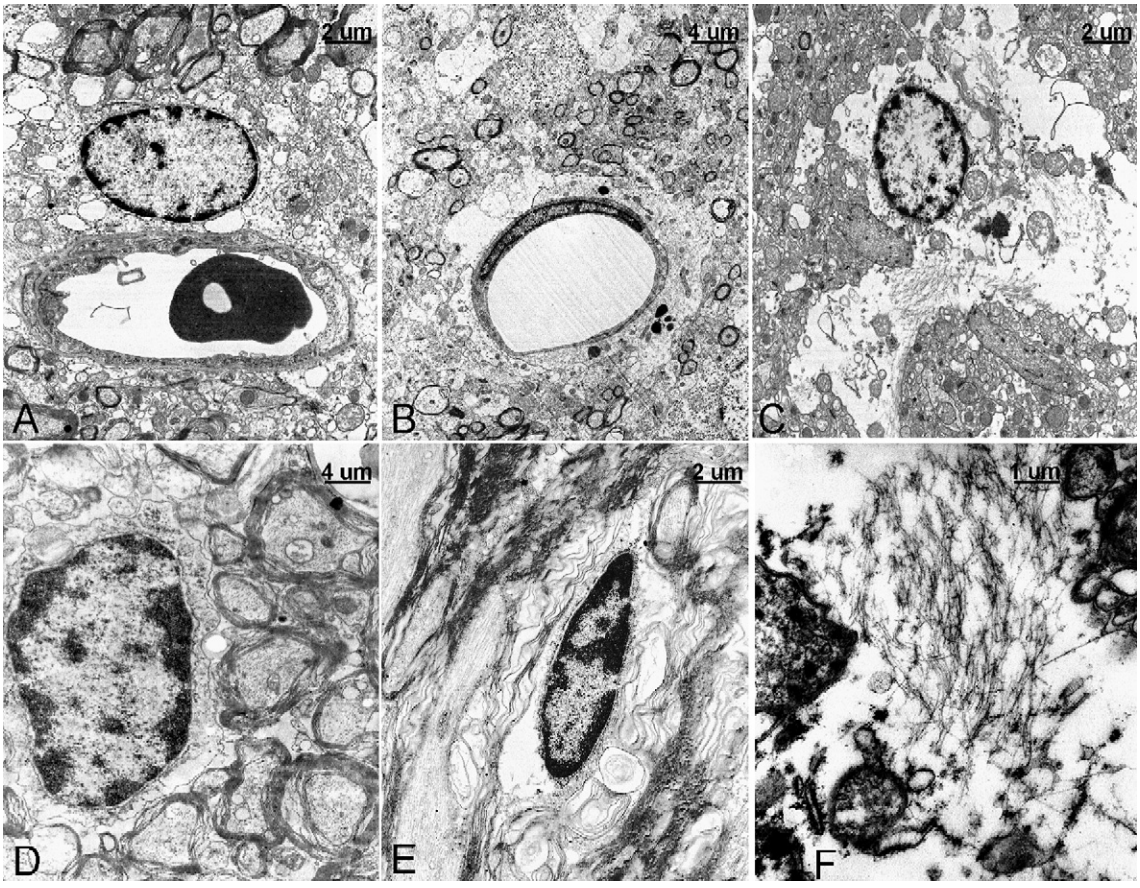

Fig. 3 – I.c.v. administration of Stx2 caused also glial ultrastructural alterations. Electron microphotographs of i.c.v. Stx2 administration next to rat corpus striatum show at the ultrastructural level a perivascular cytoplasmic astrocyte (B), a non perivascular astrocyte (C, F) and an oligodendrocyte (E–F). An astrocyte in no pathologic condition is shown (A) after an i.c.v. administration of a vehicle in the same area observed. A conserved myelin sheath from a normal oligodendrocyte (D) after i.c.v. administration of vehicle. Astrocytes in different pathologic states are shown: a perivascular one with cytoplasmic oedema (B), and another astrocyte with gliosis can be observed (C). High magnification of an astrocyte with evident gliosis in detail (F). An oligodendrocyte from a striatal fiber (E) in pathologic state.

et al., 2006). On the other hand, the elution fraction without the Stx2 did not significantly change cell viability, as compared with the cell Vero culture in RPMI medium (Fig 1C). The capacity of Stx2 to invade the brain parenchyma by passing the blood–brain barrier was previously demonstrated with tracers (Fujii et al., 1994) or by the toxin presence itself in the brain (Fujii et al., 1996). We therefore tested the capacity of Stx2 to invade the brain by i.p. administration for toxin characterization. Stx2 immunolocalization was observed in parenchymal brain cells near perivascular spaces (Fig. 1D). This was not observed by omitting primary antibody (below panel Fig. 1D) and with the incubation of an isotype antibody used as a control for the Stx2 immunohistochemistry (Saper, 2005) (above left panel Fig. 1D). The isotype chosen was the monoclonal mouse antibody raised against BrdU antigen, a molecule not present in the tissue. Because there are no reports available about the direct effect of this toxin in neurons in an in vivo model of neurological disease, we further wanted to test the toxin directly into the brain by avoiding a systemic STEC inoculation. We i.c.v. microinfused the purified toxin to the rat brain and observed by TEM whether Stx2 possesses a direct neurotoxic effect.

2.2. *Stx2 caused neuronal and fiber ultrastructural alterations in the rat corpus striatum after 8 days of i.c.v. administration*

We obtained the following electron microphotographs from ultrathin brain sections that corresponded to the dorsal caudate putamen subregion of rat corpus striatum (Fig. 2A) as shown (figure modified from Paxinos and Watson, 2005). I.c.v. microinfused brain sections with either vehicle (Fig. 2B) or Stx2 (Fig. 2C) were stained with blue toluidine to select the involved region by the toxin effect. Affected neurons in i.c.v. Stx2 microinfusions resulted to be in a more irregular and contrasted shape compared with normal ones in vehicle neurons (Figs. 2B, C). These affected neurons were identified by Stx2 immunofluorescence together with neighboring astrocytes identified by GFAP immunofluorescence (Fig. 2K). These identified areas were subsequently chosen and processed for TEM observations. In this model, Stx2 altered the ultrastructure of fibers (Fig. 2E, F) and neuronal bodies (Figs. 2H–J) in rat corpus striatum. Hypertrophic and demyelinated (Fig. 2E) sheaths of fibers could be observed. Another electron microscopy microphotograph showed an astrocyte in a position suggesting the phagocytosis of a fiber (Fig. 2F). We next wanted to determine if the direct i.c.v. administration of Stx2 caused neuronal death. Previous investigation regarding this issue is not available. In our work, electron microphotographs showed neurons in different stages of degeneration (Figs. 2H–J). One includes an apoptotic form: nuclear lateralization in a vacuolated asymmetric neuron (Fig. 2H); electrodense chromatin and nuclear fragmentation in another neuron could be observed (Fig. 2I), and in a third one a complete vacuolated contrasted cytoplasm with several electrodense ribosome-like particles (Fig. 2J). The toxin enters the cell by endocytosis and is transported through the Golgi complex en route to the endoplasmic reticulum (ER). The toxin exits the ER into the cytosol where it blocks protein translation. The A subunit is an N-glycosidase that, once

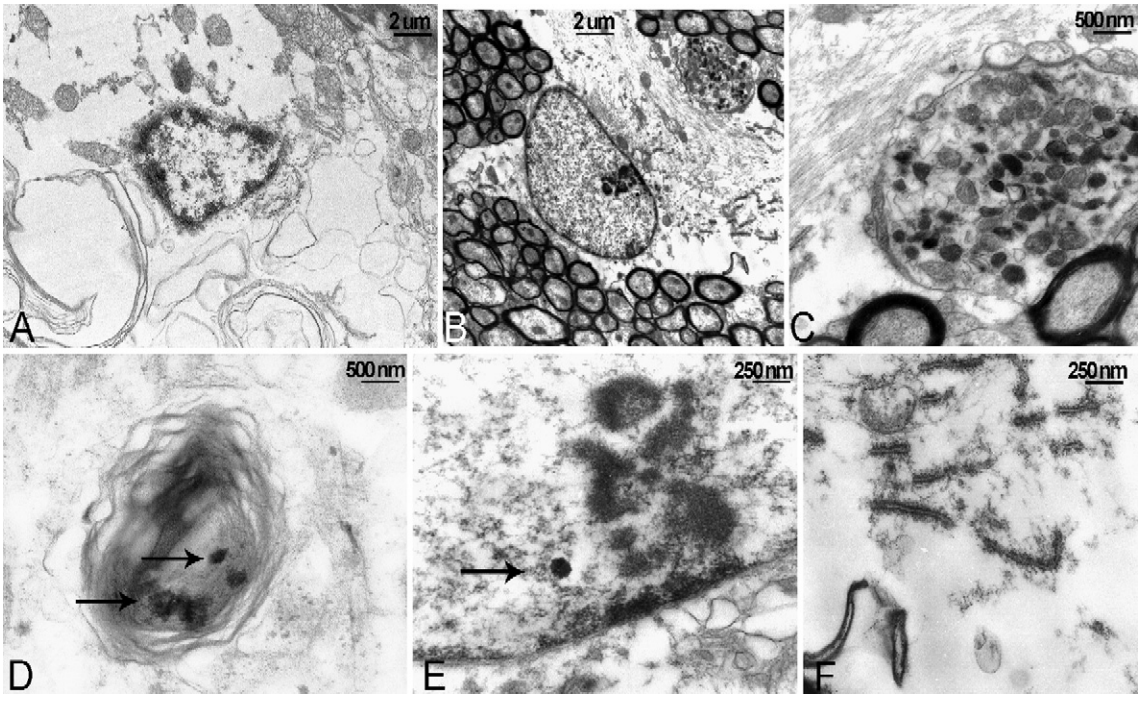

Fig. 4 – I.c.v. Stx2 administration was immunoelectron-localized in disorganized neuronal fibers and in astrocytic nucleus. DAB-clustered Stx2 immunodeposits are observed in a demyelinated axon (arrows, D) and inside the nucleus of an astrocyte (B), which can be clearly observed in a high magnification electron microphotograph (arrow, E). An isotype control performed on the same area shows demyelinated axons and an astrocyte nucleus with no observable immunodeposits (A). Immunoelectron microscopy observations are correlated with astrocytic ultrastructural changes (C, E–F). Gliosis in high magnification is observed in an astrocyte cytoplasm where an abnormal dendrite is next to it (C). F: Electrodense rough endoplasmic reticulum.

translocated into the cytosol, hydrolyzes an adenine base from ribosomal RNA (Sandvig and van Deurs, 2000). Therefore, the presence of large electrodense particles ribosome-like (Fig. 2J) could be due to a compensatory effect, as Stx2 inhibits ribosome function.

2.3. *I.c.v. Stx2 administration altered glia ultrastructure in the rat corpus striatum*

I.c.v. microinfusion of Stx2 altered the ultrastructure of oligodendrocytes and astrocytes. These were observed in injured perivascular astrocytes and oligodendrocytes by TEM (Fig. 3). Perivascular astrocyte cytoplasmic edema (Fig. 3B) and astrocyte gliofilament hypertrophy (Figs. 3C, F) were observed. Demyelinated oligodendrocytes (Fig. 3E) were also observed. Interestingly, injured astrocytes were highly observed in those that form the BBB with endothelial cells (Fig. 3B).

2.4. *Stx2 was immunoelectron-localized in astrocyte nuclei and in disorganized neuronal fibers in the rat corpus striatum after i.c.v. administration*

We next wanted to determine the Stx2 ultrastructural localization by immunoelectron microscopy in dorsal caudate putamen of the corpus striatum (Fig. 4), the area in which neuroglial damage was observed. DAB clustered immunodeposits corresponding to Stx2 were immunoelectron-detected inside demyelinated axons (Fig. 4D). The immunoelectron detection for Stx2 performed on these sections was specific, since no immunodeposits were observed outside fibers or subcellular structures (Fig. 4D). Furthermore, no DAB immunodeposits were found in isotype controls, by using an isotype primary antibody in which the correspondent antigen is not found in the experimental sample (Fig. 4A). Ultrastructural changes in a glial nucleus occurred together with Stx2 immunoelectron localization in the same nuclei of dorsal corpus striatum region (Fig. 4E). Immunoelectron detection of Stx2 on glial nuclei of the same described region was negative when sections were incubated with an isotype antibody (Fig. 4A). One of the ultrastructural changes observed was the electrodense particles in glial nuclei (Fig. 4B) with a lateralized nucleolus (Fig. 4E). At the cytoskeletal level, gliosis was observed in the same cell (Fig. 4C) together with an electrodense rough endoplasmic reticulum (Fig. 4F). A neighbor dendrite with high content of augmented protein densities and mitochondria claimed for a dendrite in pathologic state (Fig. 4C).

3. Discussion

Consistent with previous findings by other authors that systemic administration of Stx2 could cause brain damage in different models of animals (Fujii et al., 1996; Mizuguchi et al., 2001) or infected with STEC (Kita et al., 2000; Okayama et al., 2004) in this study we moved forward to understand the role of Stx2 in the brain. We found strong evidence supporting the hypothesis that the i.c.v. administration of this toxin is directly involved in rat brain damage by affecting neuronal and glial cells of corpus striatum. This approach discarded the synergistic effect of Stx2 with pro-inflammatory cytokines TNF-α and IL-1β, produced on endothelial cells (Paton and Paton, 1998). TNF-α increase was observed in mice brain homogenates after STEC infection (Okayama et al., 2004). However this action was not expected in the i.c.v. model of brain damage because Stx2 was not injected in the systemic vasculature but rather in the brain lateral ventricle. We precisely did not observe endothelial brain damage. Instead we found astrocytes with intracytoplasmic edema and gliosis when the toxin diffused into the brain parenchyma. This is probably the reason why Stx2 does not reach the microvasculature. Therefore this i.c.v. method is useful to study the direct damage of Stx2 in neurons and glial cells without the involvement of pro-inflammatory systemic cytokines or other neurotoxic systemic elements.

The Stx2 used in the i.c.v. microinfusion was the end product of a supernatant cell culture by which proteins were subsequently precipitated, dialyzed and passed through an affinity chromatography column. We found that the purified Stx2 resulted to be cytotoxic to Vero cells in a similar dose found in another report (Karmali et al., 1985). In addition, Stx2 was able to bypass the BBB, by which this pathophysiologic feature is supported by other authors (Fujii et al., 1996). Stx2 was immunolocalized in cells near perivascular regions after i.p. administration.

After 8 days of i.c.v. Stx2 microinfusion, ultrastructural alterations of fibers and neuronal bodies in the rat corpus striatum were observed. These changes included different stages of neuronal degeneration, hypertrophic and demyelinated axon fibers and were correlated with the immunoelectron localization of Stx2 in demyelinated axons and with the endoplasmic reticulum reaction of neurons. Therefore the presence of Stx2 in striatal neurons detected by immunoelectron microscopy labeling showed to be neurotoxic in vivo. Stx2 immunoelectron detection was also observed on astrocyte nuclei. It was postulated that Stx2B may be involved in inhibiting rRNA assembly (Falguieres and Johannes, 2006). Therefore, its presence may cause alterations at the ultrastructural level in this compartment. The i.c.v. administration of Stx2 caused also cytoplasmic edema and gliosis, and demyelinated sheaths in oligodendrocytes.

Striatal neurons may express a receptor for the toxin. Neuronal apoptosis may be caused by the action of endocytosed Stx2. The neuronal presence of Stx glycolipid receptors was described in dorsal root ganglion neurons (Ren et al., 1999). However, the presence of a Gb3 receptor in striatum neurons was not yet described and the finding of an in vivo Stx2 neuronal or glial receptor is yet an issue to be addressed.

In our work, we observed that is the Stx2 itself the consequence of neuronal brain damage. How the toxin acts inside the neuron remains to be elucidated. A fundamental issue to be addressed is whether the toxin alters neurotransmitter neuronal metabolism. One possibility to remark would be the action of Stx2 in the synthesis of nitric oxide (NO) in some subsets of striatal neurons. We previously observed the neuronal alteration in the synthesis of NO after a neuronal damage (Goldstein et al., 1997). Which could be the factor that triggered this phenomenon? As far as we know, there is no information regarding this and this remains an open question.

The main input structure of the basal ganglia is the striatum (Gerfen, 2004), which is specifically related to limb movements in its dorsolateral area and it extends between AP +1.6 mm to −1.0 mm relative to bregma (West et al., 1990). These coordinates are coincident with our i.c.v. stereotaxic Stx2 microinfusion. Then i.c.v. administration could be a valid method to study the Stx2 behavior on rat striatum.

The present work showed the first animal model of i.c.v. administration of Stx2 as far as we know. Also, this was the first brain model of Stx2 administration performed in rats. The i.c.v. technique allowed to microinfuse the toxin in specific brain areas of interest by using a stereotaxic frame. We placed the cannula between the third and lateral ventricles, in contact with the corpus striatum to avoid tissue damage. This is very different from i.p. or e.v. toxin administrations because the distance of delivery is too far to assume direct effects of the toxin in the brain. The toxic induction of systemic pro-inflammatory responses by Stx has also been reported. One of these responses is the rapid induction of TNF-α after STEC infection in mice with protein calorie malnutrition (Kita et al., 2000). Therefore the i.c.v. technique enables us to study the direct effect of the toxin in corpus striatum disregarding the involvement of systemic secondary responses. A previous report showed intrathecal Stx administration in rabbit cisterna magna (Fujii et al., 1998), located between the medulla and the cerebellum; this approach to study the direct action of Stx2 in the CNS may be valid to study the action of the toxin in cerebellum, pons and medulla, but may not be for specific areas of the brain. Whether other striatum local potential partners of action may synergistically play together with Stx2 brain injury, remains to be considered.

As a novel finding, we showed a detailed ultrastructural study of the Stx2 action when it was i.c.v. microinfused in the rat brain. Apoptotic neurons observed by TEM, in association with Stx2 immunoelectron labeling, together with pathological ultrastructural alterations of astrocytes and oligodendrocytes were observed in the affected areas. All the presented data clearly demonstrated the direct neurotoxic involvement of Stx2 in particular brain areas which would be involved in CNS damages observed in children with HUS.

4. Experimental procedures

4.1. *Stx2 plasmid*

Standard techniques were used to construct an expression plasmid (Sambrook et al., 1989). The plasmid was isolated from the bacteria using the Wizard Plus SV miniprep DNA purification system (Promega Corp., Madison, WI, USA). The construct was sequenced by the dideoxy chain-termination method using an Applied Biosystem automatic sequencer. The *stx2a* and *stx2b* genes were obtained from chromosomal DNA of *E. coli* C600 containing the 933W bacteriophage (22) (a gift from M. Rivas, Instituto Nacional de Enfermedades Infecciosas "Dr. Carlos G. Malbrán", Buenos Aires, Argentina). A fragment of 1422 bp was amplified by the polymerase chain reaction (PCR) from chromosomal DNA using two specific primers (upstream: 5′-GAA TTC ATT ATG CGT TGT TAG-3′ and downstream: 5′-GAA TTC TCA GTC ATT ATT AAA CTG-3′, both containing an *Eco*RI restriction site) flanking both the *stx2a* and *stx2b* genes. The PCR product was cloned into pGEM-T Easy (Promega Corp., Madison, WI, USA). Competent *E. coli* DH5α cells (Life Technologies, Rockville, MD, USA) were transformed and the isolated plasmid was designated pStx2.

4.2. *Stx2 purification*

Stx2 was purified by affinity chromatography under native conditions. Briefly, recombinant *E. coli* DH5α containing pStx2 were cultured in LB supplemented with 100 μg/ml ampicillin until an OD_{600} of 0.6. The bacterial pellet obtained after centrifugation at 6000 rpm for 10 min was resuspended in lysis buffer (50 mM NaH_2PO_4, 300 mM NaCl, pH 8) and incubated on ice for 30 min. The suspension was then sonicated, centrifuged at 12,000 rpm for 20 min, and the supernatant was precipitated with a saturated solution of $SO_4(NH_4)_2$ following precipitation at 12,000 rpm at 4 °C for 20 min. The pellet containing the Stx2 was resuspended in the preceded lysis buffer and dialyzed against 8.1 mM Na_2HPO_4, 1.5 mM $NaH_2PO_4{\cdot}H_2O$, 137 mM NaCl, 2.7 mM KCl to remove $SO_4(NH_4)_2$ to be subsequently washed and eluted for affinity chromatography in an agarose–galabiose resin (Calbiochem, La Jolla, CA). The dialyzed Stx2 A and B subunits adhered to the galabiose portion of the resin (Tarragó-Trani and Storrie, 2004; Tomada et al., 2002). The resin was subsequently washed with 10 mM PBS, 10 mM $NaH_2PO_4{\cdot}H_2O$, 10 mM $NaH_2PO_4{\cdot}H_2O$ containing 1 M NaCl. Finally, the complete holotoxin Stx2 were eluted with 50 mM $NaH_2PO_4{\cdot}H_2O$, containing 0.5 M melibiose (Sigma, St. Louis, MO, USA). All the preceding solutions were in pH=7.0. To determine the Stx2 purity, all fractions were diluted in loading buffer, separated on a 12.5% SDS polyacrylamide gel, electrotransferred to nitrocellulose membrane (Hybond ECL, Amersham Pharmacia Biotech, Buckinghamshire, UK) and immunoblotted with either a monoclonal anti-verotoxin II (slt-2B) or either with a monoclonal anti-verotoxin II (slt-2A) (Biodesign International, ME, USA) directed against the B or A subunits of Stx2. The first eluted fraction showed two bands of approximately 32 kDa and 7.7 kDa that corresponded to the A and B complete Stx2 subunits as shown in Coomassie blue stained SDS–PAGE gels and also in Western blot. An eluted fraction without Stx2 was used as the vehicle. The quantity of the Stx2 purification was determined by the Bradford method. This purification procedure resulted in approximately 1 ng/μl Stx2.

4.3. *Characterization of the Stx2 purification in Vero cells*

The first eluted fraction that contained the Stx2 was assayed for toxicity to Vero cells (Karmali et al., 1985) by neutral red assay. The neutral red cytotoxicity assay was adapted from previously described protocols (Karpman et al., 1998). Vero cells were plated in 96-well plates and grown to confluence in complete RPMI medium. The cells were then washed in PBS and exposed to different concentrations 10^{-8} pg/ml to 10^{6} pg/ml Stx2 holotoxin in growth-arrested conditions for 72 h. 200 μl of freshly diluted neutral red in RPMI medium was added to a final concentration of 50 μg/ml and cells were incubated for additional 3 h at 37 °C in CO_2 incubator at 5%.

Cells were then washed with a solution that contained 200 μl of $CaCl_2$ 1%, formaldehyde 4% twice and then, they were solubilized in 200 μl of acetic acid 1% in ethanol 50%. Absorption in each well was read in an automated plate spectrophotometer at 546 nm. Results were expressed as neutral red uptake percent, and 100% represents cells incubated under identical conditions but without toxin treatment. The 50% cytotoxic dose (CD_{50}) corresponded to the dilution required to kill 50% of Vero cells. For neutralization assay of Stx2 eluted fractions Vero cells were grown as previously described. 0.1, 10 and 1000 pg/ml of the Stx2 eluted fraction were mixed with 50 ng/ml or 5 μg/ml of the monoclonal Stx2B antibody (Slt-2B, Biodesign International) for about 30 min at 37 ° C, in shaking. This cocktail was then incubated with the Vero cell culture for 24 h. Vero cell viability and cytotoxicity were assay by using the neutral red technique as described previously. Neutralization controls were performed by omitting either Stx2, the antibody anti-Stx2, or both.

In order to determine the capacity of Stx2 to bypass the rat BBB, rats were i.p. injected with the toxin. After 48 h, rats were perfused with a fixative solution (procedure detailed below). Brain floating sections were subjected to immunohistochemistry to localize Stx2. Brain sections were rinsed several times in 10 mM PBS, and then incubated for 20 min with 0.3% H_2O_2 diluted in methanol to prevent endogenous peroxidase activity. Brain sections were then rinsed several times in 10 mM PBS and further incubate with 2.5% normal donkey serum for 40 min. The sections were further incubated for 72 h at 4 °C with a mouse monoclonal Stx2B antibody (1:50, slt-2B, Biodesign International). Negative controls were performed by omitting the primary antibody. The mouse monoclonal anti-BrdU (dilution 1:50, clone DU 33 #B 2531, Sigma, St. Louis, MO, USA) immunohistochemistry was used as an isotype control. After several rinses in 10 mM PBS, the sections were incubated with a secondary antibody (RTU Vectastain Elite ABC reagent kit, Vector Laboratories, Burlingame, CA) and developed using DAB (Vector Laboratories). After several rinses in 10 mM PBS, the sections were mounted on glass slides, dehydrated and cover slipped with mounting media.

4.4. *Animals*

250–300 g male Sprague–Dawley rats were housed in air-conditioned and light-controlled (lights between 06:00 and 18:00 h) animal house. They were provided with food and water ad libitum. After 8 days of i.c.v. Stx2 or vehicle infusions, the rats were sacrificed for ultrastructural studies. Rats were anesthetized with sodium pentobarbital (60 mg/kg) and perfused transcardially with 0.9% NaCl solution followed by 4% paraformaldehyde and 0.25% glutaraldehyde in 0.1 M phosphate buffer (PB) [fixative per animal weight (ml/g)]. Brains were removed from skull, post-fixed in the same fixative solution for 2 h. All these procedures were performed according to regular protocols (Lopez-Costa et al., 1994, Priestley et al., 1992). Brain sections were cut on an Oxford vibratome. Serial 40-μm-thick coronal sections were obtained and collected in 0.1 M phosphate buffer. Brain floating sections obtained were processed either for light microscope blue toluidine staining or for ultrathin slices to immunoelectron microscope studies. The experimental protocols and euthanasia procedures were reviewed and approved by the Institutional Animal Care and Use Committee of University of Buenos Aires.

4.5. *I.c.v. infusion of Stx2*

Anaesthetized rats (ketamine 50 mg/kg – diazepam 0.35 mg/kg, i.p.) were stereotaxically implanted onto the joint of the lateral and third ventricles with a stainless steel guide cannula (Plastic One, Roanoke, VA). The placement coordinates were anteroposterior: −0.96 mm; lateral: 2 mm and vertical: 3.2 mm (Paxinos and Watson, 2005). To reach the ventricle area and minimize the damage of tissue, a 21-gauge guide cannula was implanted at this point. Then, a 30-gauge needle that extends 0.5 mm below the guide cannula was used for the injections. Correct placement of the ventricle cannulae was verified at the end of the experiment, followed by postmortem brain fixation and cut on an Oxford vibratome; data obtain from improperly implanted animals were excluded from analysis. Cannulae were fixed to the skull surface with three screws and dental acrylic cement and temporarily occluded with dummy cannulae. After surgery, animals were caged individually. Rats were randomly assigned to different experimental groups and each rat was used only once. 1 week after on the day of the experiment, the i.c.v. injection was made in freely moving animals through a 30-gauge needle connected by polyethylene tubing to a 20-μl Hamilton syringe. The needle was left in place for 30 s to prevent back flow of the injected solution. The rats were i.c.v. injected with 6 μl of vehicle or 6 μl of Stx2 (1 ng/μl). After 8 days, the rats were sacrificed for ultrastructural studies.

4.6. *TEM and immunoelectron cytochemistry*

For immunoelectron cytochemistry brain floating sections were rinsed in 10 mM PBS, and then incubated for 20 min in PBS containing 5% normal donkey serum. Sections were incubated for 48 h at 4 °C with the monoclonal anti-Stx2B antibody (Biodesign International) (1:100). Controls were performed by an isotype control using the monoclonal anti-BrdU (clone DU 33 #B 2531, Sigma, St. Louis, MO, USA). After several rinses in PBS, the sections were incubated with a secondary donkey anti-mouse antibody (1:100) coupled with peroxidase (Vector Laboratories) diluted in PBS for 1 h. After several rinses in PBS, the sections were developed with a solution containing 0.05 % DAB and 0.01 % H_2O_2 in 10 mM PBS, pH=7.4 for 10 min. The sections were subsequently processed for TEM observation. The samples were first assessed by light microscopy with blue toluidine to select the areas for TEM studies. Ultrathin sections were cut from selected areas (Priestley et al., 1992). Ultrathin sections were contrasted with 1% OsO_4 and 1% uranyl acetate, dehydrated and flat-embedded in Durcupan. The sections were contrasted with lead citrate, examined and photographed on a Zeiss 109 electron microscope. Adobe Photoshop software was used in the assembly of images (Adobe Systems Inc., San Jose, CA, USA).

4.7. *Visualization of Stx2 and GFAP*

Brain floating sections were incubated with BSA 1%+ monoclonal anti-Stx2B antibody (1/50) for 48 h at 4 °C, following

incubation for 1 h with goat IgG anti-mouse/FITC (1:100) (Sigma, St. Louis, MO, USA) in PBS and incubated with 1% BSA for 1 h; a polyclonal rabbit antibody against GFAP (Sigma, St. Louis, MO, USA) (1:500) was diluted in 10 mM PBS+0.2% TX, incubated for 48 h at 4 °C. After that, a secondary goat IgG anti-rabbit Cy3 (Zymed Laboratories Inc, San Francisco, CA, USA) (1:100) was incubated for 1 h in 10 mM PBS. After several washes with PBS, the floating sections were mounted on glass slides and cover slipped in fluorescence mounting solution (Vectashield, Vector Laboratories). Controls were performed using the same procedure but omitting the primary antibody or by using an isotype control described above. For visualization of the i.c.v. microinfusion of eluted Stx2, a green fluorescence filter was used, and for GFAP the filter was shifted to red. Confocal colocalization images were performed by Gray-scale images (12 bit), acquired with an Olympus FV300 microscope using the green helium–neon laser (543 nm) and argon laser (488 nm). Images were captured with Fluo View application software. Serial optical sections were performed with Simple 32 C-imaging computer. Z-series sections were collected at 1 μm with a UplanApo 40×. A scan zoom of ×1 was used in the acquisition of images. Adobe Photoshop software was used in the assembly of images. Merge images were obtained using this program.

4.8. *Image processing*

For visualization of brain sections stained with blue toluidine or immunohistochemistry of anti-Stx2 developed with DAB–peroxidase system a microscope Nikon Eclipse 2000 was used (Nikon Instruments Inc., Melville, NY, USA). Images were captured with a Nikon Coolpix 4300 digital camera (Nikon Corporation, Tokyo, Japan). Adobe Photoshop software was used in the assembly of images (Adobe Systems Inc., San Jose, CA, USA).

4.9. *Statistical analysis*

Five brain sections from six animals for i.c.v. Stx2 microinfusion and the same number for the vehicle condition were used for TEM studies. Five brain sections from five independent immunoelectron cytochemistry experiments in each condition were used for Stx2 striatal localization. For Stx2 characterization, data shown are mean±S.E.M. The statistical significance between two mean values obtained for two different experimental conditions was calculated by the Student's *t*-test. All data from the curves were analyzed by one-way analysis of variance (ANOVA). *P* values <0.05 were considered significant. For BBB characterization, five sections from three rats were used.

Acknowledgments

These studies were supported by CONICET (National Research Council) grant PIP5588 to J. G. and Fondo Nacional para la Ciencia y la Tecnología grant FONCYT-PICT 26224, CONICET grant PIP 5587 and Universidad de Buenos Aires (UBA) grant UBACYT M038 to C. I. We would like to thank Mariana Lopez Ravasio of Laboratorio Nacional de Investigación y Servicios en Microscopía Electrónica (LANAIS-MIE)/CONICET, who assisted us in the processing of the brain tissue for transmission electron microscopy study. Electron microscopy was carried out at the LANAIS-MIE from the UBA-CONICET.

REFERENCES

Barnett, N.D.P., Kaplan, A.M., Bernes, S.M., Cohen, M.L., 1995. Hemolytic uremic syndrome with particular involvement of basal ganglia and favorable outcome. Pediatr. Neurol. 12, 155–158.

Eriksson, K.J., Boyd, S.G., Tasker, R.C., 2001. Acute neurology and neurophysiology of haemolytic–uraemic syndrome. Arch. Dis. Child. 84, 434–435.

Exeni, R.A., 2001. Sindrome urémico hemolítico. Arch. Latin Nefr. Ped. 1, 35–56.

Falguieres, T., Johannes, L., 2006. Shiga toxin B-subunit binds to the chaperone BiP and the nucleolar protein B23. Biol. Cell 98, 125–134.

Fujii, J., Kita, T., Yoshida, S., Takeda, T., Kobayashi, H., Nakata, N., Ohsato, K., Mizuguchi, Y., 1994. Direct evidence of neuron impairment by oral infection with verotoxin-producing *Escherichia coli* O157:H– in mitomycin-treated mice. Infect. Immun. 62, 3447–3453.

Fujii, J., Kinoshita, Y., Kita, T., Higure, A., Takeda, T., Tanaka, N., Yoshida, S., 1996. Magnetic resonance imaging and histopathological study of brain lesions in rabbits given intravenous verotoxin 2. Infect. Immun. 64, 5053–5060.

Fujii, J., Kinoshita, Y., Yamada, Y., Yutsudo, T., Kita, T., Takeda, T., Yoshida, S., 1998. Neurotoxicity of intrathecal Shiga toxin 2 and protection by intrathecal injection of anti-Shiga toxin 2 antiserum in rabbits. Microb. Pathog. 25, 139–146.

Gallo, E.G., Gianantonio, C.A., 1995. Extrarenal involvement in diarrhoea-associated haemolytic–uraemic syndrome. Pediatr. Nephrol. 9, 117–119.

Gerfen, C.R., 2004. Basal ganglia, In: Paxinos, G. (Ed.), The Rat Nervous System, third edition. Elsevier Academic Press, London, pp. 455–508.

Goldstein, J., Lopez-Costa, J.J., Pecci Saavedra, J., 1997. Changes in NADPH–diaphorase reactivity and neuronal nitric oxide synthase in the rat retina following constant illumination. Neurosci. Lett. 231, 45–48.

Karmali, M.A., Petric, M., Lim, C., Cheung, R., Arbur, G.S., 1985. The association between hemolytic uremic syndrome and infection by Verotoxin producing *Escherichia coli*. J. Inf. Disp. 151, 775–782.

Karpman, D., Hakansson, A., Perez, M.T., Isaksson, C., Carlemalm, E., Caprioli, A., Svanborg, C., 1998. Apoptosis of renal cortical cells in the hemolytic–uremic syndrome: in vivo and in vitro studies. Infect. Immun. 66, 636–644.

Kita, E., Yunou, Y., Kurioka, T., Harada, H., Yoshikawa, S., Mikasa, K., Higashi, N., 2000. Pathogenic mechanism of mouse brain damage caused by oral infection with Shiga toxin-producing *Escherichia coli* O157:H7. Infect. Immun. 68, 1207–1214.

Lopez-Costa, J.J., Averill, S., Pang Ching, Y., Priestley, J.V., 1994. Immunocytochemical localization of a growth-associated protein (GAP-43) in rat adrenal gland. Cell Tissue Res. 275, 555–566.

Mizuguchi, M., Tanaka, S., Fujii, I., Tanizawa, H., Suzuki, Y., Igarashi, T., Yamanaka, T., Takeda, T., Miwa, M., 1996. Neuronal and vascular pathology produced by verocytotoxin 2 in the rabbit central nervous system. Acta Neuropathol. 91, 254–262.

Mizuguchi, M., Sugatani, J., Maeda, T., Momoi, T., Arima, K.,

Takashima, S., Takeda, T., Miwa, M., 2001. Cerebrovascular damage in young rabbits after intravenous administration of Shiga toxin 2. Acta Neuropathol. 102, 306–312.
Oakes, R.S., Siegler, R.L., McReynolds, M.A., Pysher, T., Pavia, A.T., 2006. Predictors of fatality in postdiarrheal hemolytic uremic syndrome. Pediatrics 117, 1656–1662.
O'Brien, A.D., Kaper, J.B., 1998. Shiga toxin-producing *Escherichia coli*: yesterday, today, and tomorrow. In: Kaper, J.B., O'Brien, A.D. (Eds.), *Escherichia coli* O157:H7 and Other Shiga Toxin-Producing *E. coli* Strains. . Am. Soc. Microbiology. Washington, DC, pp. 1–11.
Okayama, A., Mikasa, K., Matsui, N., Higashi, N., Miyamoto, M., Kita, E., 2004. An interventional approach to block brain damage caused by Shiga toxin-producing *Escherichia coli* infection, by use of a combination of phosphodiesterase inhibitors. J. Inf. Disp. 190, 2129–2136.
Paton, J.C., Paton, A.W., 1998. Pathogenesis and diagnosis of Shiga toxin-producing *Escherichia coli* infections. Clin. Microbiol. Rev. 11, 450–479.
Paxinos, G., Watson, C., 2005. The Rat Brain in Stereotaxic Coordinates, fifth edition. Elsevier Academic Press, Burlington, MA, USA.
Pistone Creydt, V., Silberstein, C., Zotta, E., Ibarra, C., 2006. Cytotoxic effect of Shiga Toxin-2 holotoxin and its B subunit on human renal tubular epithelial cells. Microbes Infect. 8, 410–419.
Priestley, J.V, Alvarez, F.J., Averill, S., 1992. Pre-embedding electron microscopic immunocytochemistry. In: Polak, J.M., Priestley, J.V. (Eds.), Electron Microscopic Immunocytochemistry. Oxford University Press, Oxford, pp. 89–121.
Proulx, F., Seidman, E.G., Karpman, D., 2001. Pathogenesis of Shiga toxin-associated hemolytic uremic syndrome. Pediatr. Res. 50, 63–171.
Ren, J., Utsunomiya, I., Taguchi, K., Ariga, T., Tai, T., Ihara, Y., Miyatake, T., 1999. Localization of verotoxin receptors in nervous system. Brain Res. 825, 183–188.
Repetto, H.A., 2005. Long-term course and mechanisms of progression of renal disease in hemolytic uremic syndrome. Kidney Int. 68 (Suppl. 97), S102–S106.
Sambrook, J., Fritsch, E.F., Maniatis, T., 1989. Molecular Cloning: A Laboratory Manual. Cold Spring Harbor Laboratory Press, Cold Spring Harbor, NY, USA.
Sandvig, K., van Deurs, B., 2000. Entry of ricin and Shiga toxin into cells: molecular mechanisms and medical perspectives. EMBO J. 19, 5943–5950.
Saper, C.B., 2005. An open letter to our readers on the use of antibodies. J. Comp. Neurol. 493, 477–478.
Siegler, R.L., 1994. Spectrum of extrarenal involvement in postdiarrheal hemolytic–uremic syndrome. J. Pediatr. 125, 511–518.
Steinborn, M., Leiz, S., Rüdisser, K., Griebel, M., Harder, T., Hahn, H., 2004. CT and MRI in haemolytic uraemic syndrome with central nervous system involvement: distribution of lesions and prognostic value of imaging findings. Pediatr. Radiol. 34, 805–810.
Stricklett, P.K., Hughes, A.K., Ergonul, Z., Kohan, D.E., 2002. Molecular basis for up-regulation by inflammatory cytokines of Shiga toxin 1 cytotoxicity and globotriaosylceramide expression. Infect Dis. 186, 976–982.
Tarrago-Trani, M.T., Storrie, B., 2004. A method for the purification of Shiga-like toxin 1 subunit B using a commercially available galabiose–agarose resin. Protein Expr. Purif. 38, 170–176.
Taylor Jr., F.B., Tesh, V.L., DeBault, L., Li, A., Chang, A.C., Kosanke, S.D., Pysher, T.J., Siegler, R.L., 1999. Characterization of the baboon responses to Shiga-like toxin: descriptive study of a new primate model of toxic responses to Stx-1. Am. J. Pathol. 154, 1285–1299.
Tomada, H., Arai, M., Koyama, N., Matsui, H., Omura, S., Obata, R., Lee, Y.C., 2002. Purification of Shiga-like toxin 1 by pigeon egg white glycoproteins immobilized on sepharose gels. Anal. Biochem. 311, 50–56.
West, M.O., Carelli, R.M., Pomerantz, M., Cohen, S.M., Gardner, J.P., Chapin, J.K., Woodward, D.J., 1990. A region in the dorsolateral striatum of the rat exhibiting single-unit correlations with specific locomotor limb movements. J. Neurophysiol. 64, 1233–1246.
Yamada, Y., Fujii, J., Murasato, Y., Nakamura, T., Hayashida, Y., Kinoshita, Y., Yutsudo, T., Matsumoto, T., Yoshida, S., 1999. Brainstem mechanisms of autonomic dysfunction in encephalopathy-associated Shiga toxin 2 intoxication. Ann. Neurol. 45, 716–723.